Electronic Supplementary Material (ESI) for Industrial Chemistry & Materials.

Supporting Information

Tunable construction of CuS nanosheets@flower-like ZnCo-layered double hydroxide nanostructures for hybrid supercapacitor

Akbar Mohammadi Zardkhoshoui*, Ramtin Arian, and Saied Saeed Hosseiny Davarani*

Department of Chemistry, Shahid Beheshti University, G. C., 1983963113, Evin, Tehran, Iran.

Corresponding authors: *Tel: +98 21 22431661; Fax: +98 21 22431661; E-mail: ss-hosseiny@sbu.ac.ir (S.S.H. Davarani); and mohammadi.bahadoran@gmail.com (A. Mohammadi Zardkhoshoui)

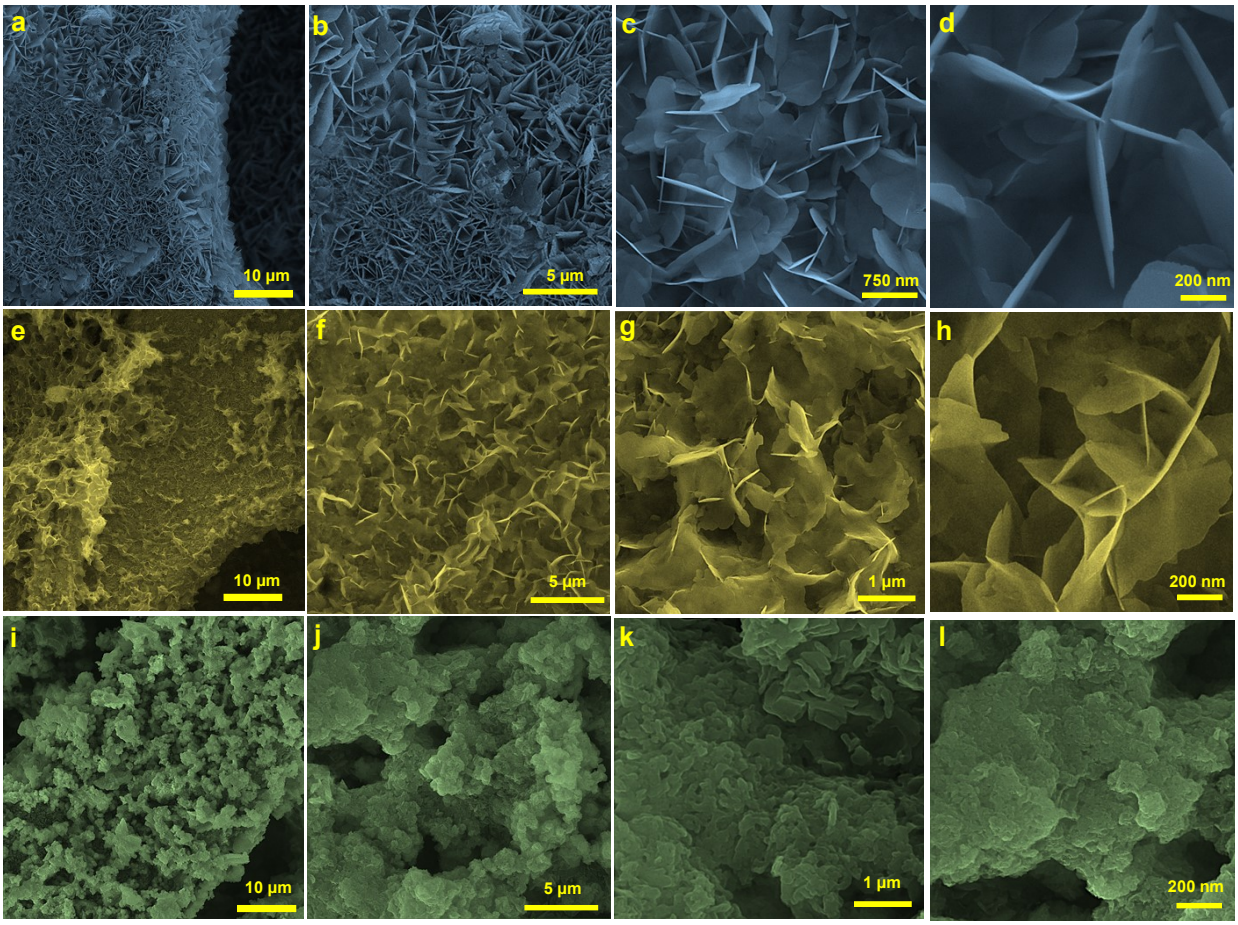

Fig. S1 (a-d) FE-SEM images of the NF@CS5. (e-h) FE-SEM images of the NF@CS10. (i-l) FE-SEM images of the NF@CS15.

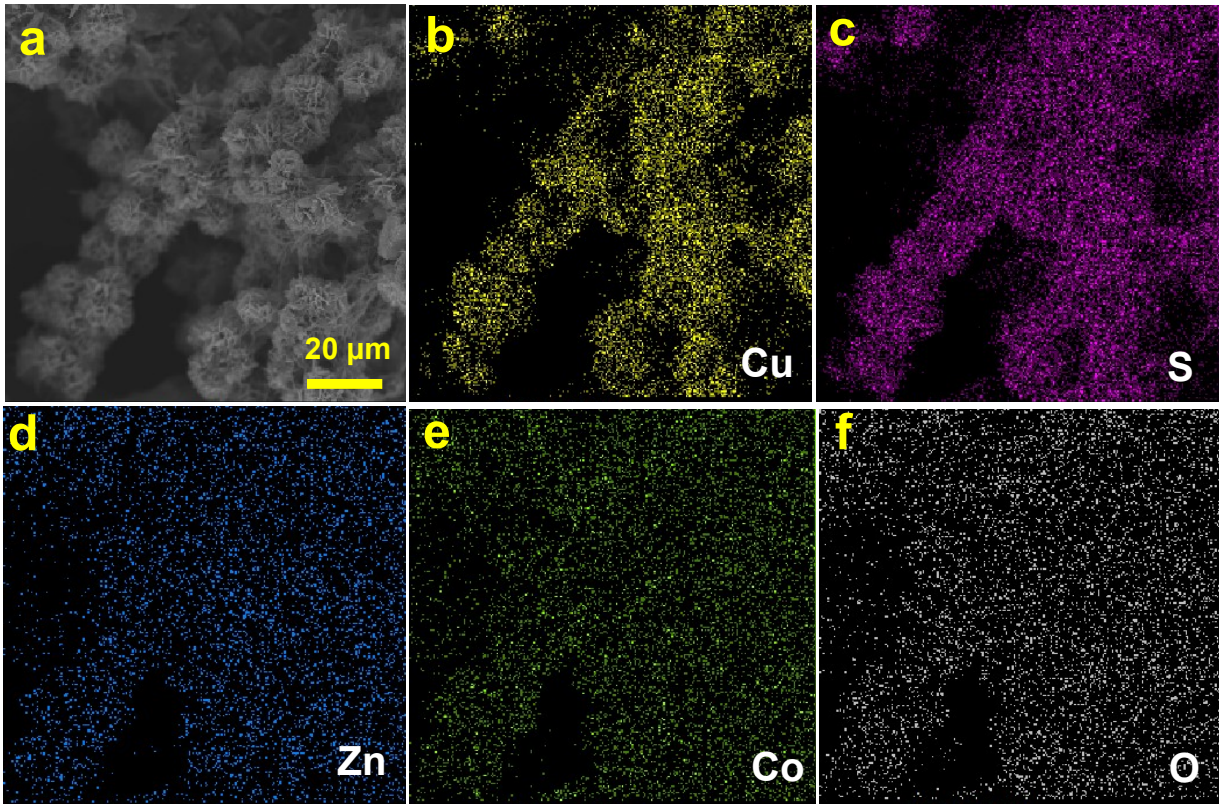

Fig. S2 (a-f) FE-SEM mapping images of the NF@CS10-ZC-LDH4.

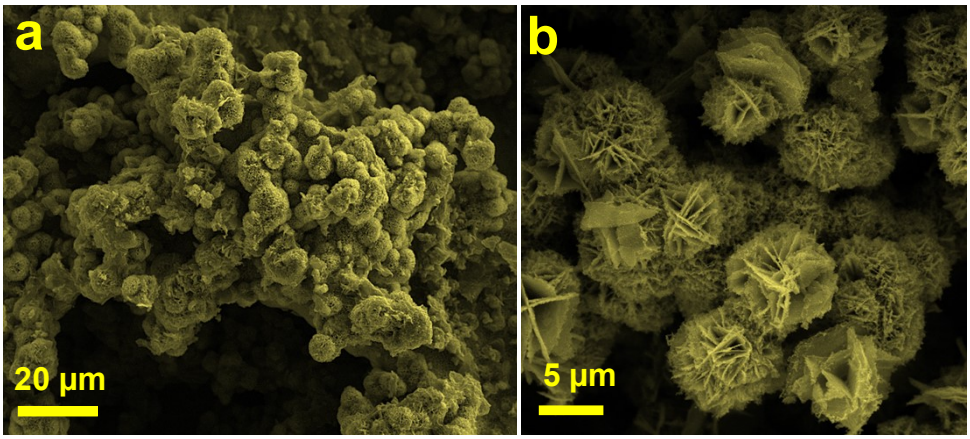

Fig. S3 (a, b) FE-SEM images of the pure NF@ZC-LDH4.

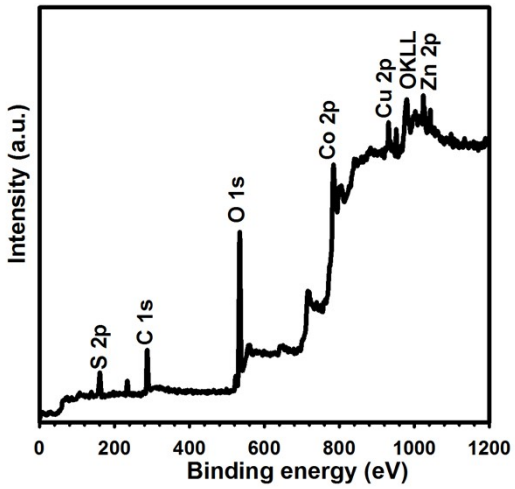

Fig. S4 XPS survey of the CS10-ZC-LDH4 sample.

.

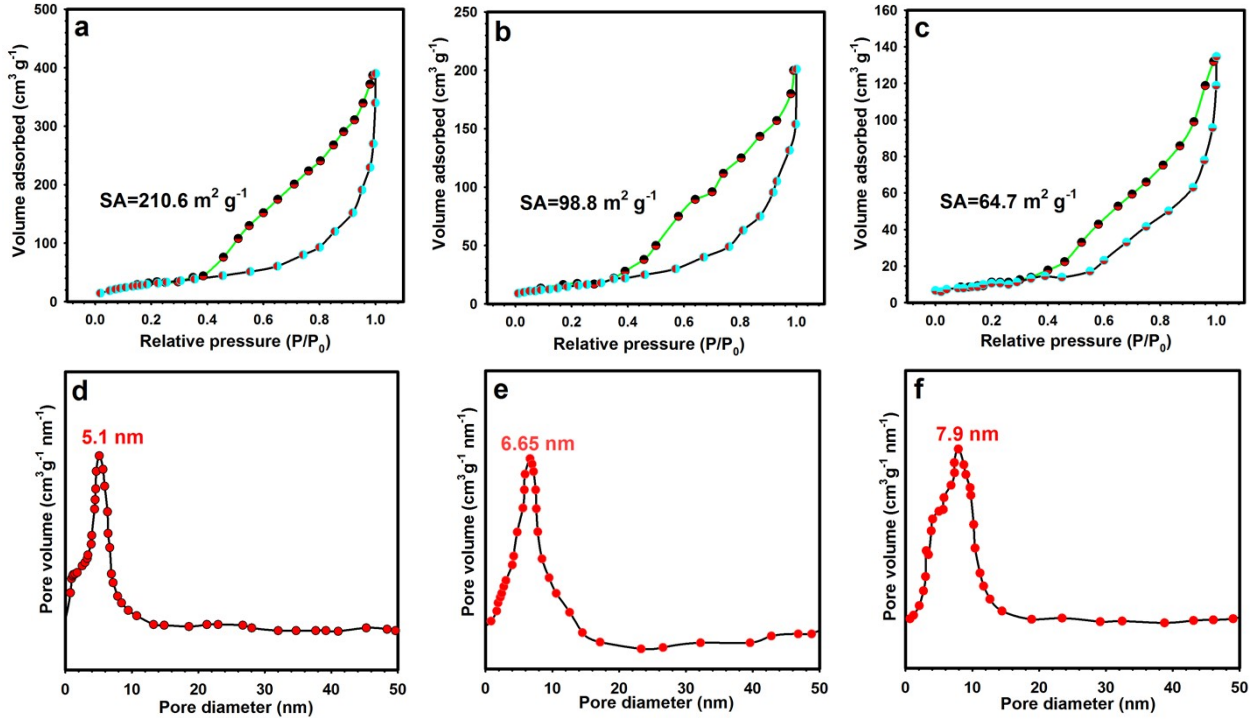

Fig. S5 (a) BET curve of the CS10-ZC-LDH4. (b) BET curve of the ZC-LDH4. (c) BET curve of the CS10. (d) BJH plot of the CS10-ZC-LDH4. (e) BJH plot of the ZC-LDH4. (f) BJH plot of the CS10.

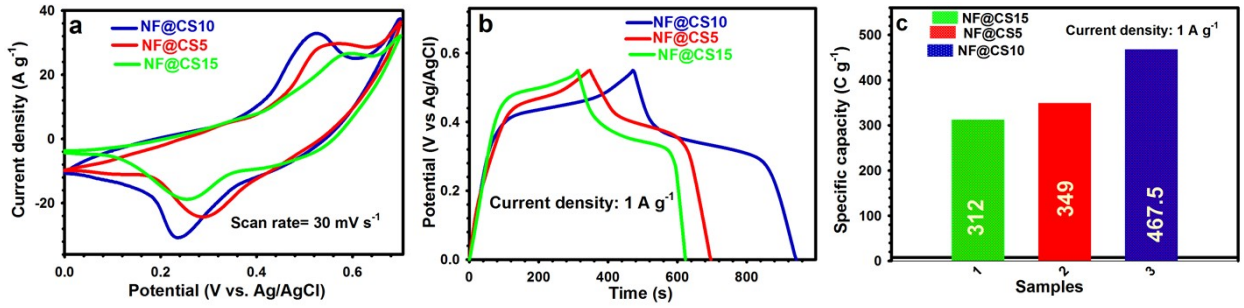

Fig. S6 (a) CV plots of the NF@CS5, NF@CS10, and NF@CS15 electrodes at 30 mV s^{-1}. (b) GCD curves of the NF@CS5, NF@CS10, and NF@CS15 electrodes at 1 A g^{-1}. (c) Specific capacities of the NF@CS5, NF@CS10, and NF@CS15 electrodes at 1 A g^{-1}.

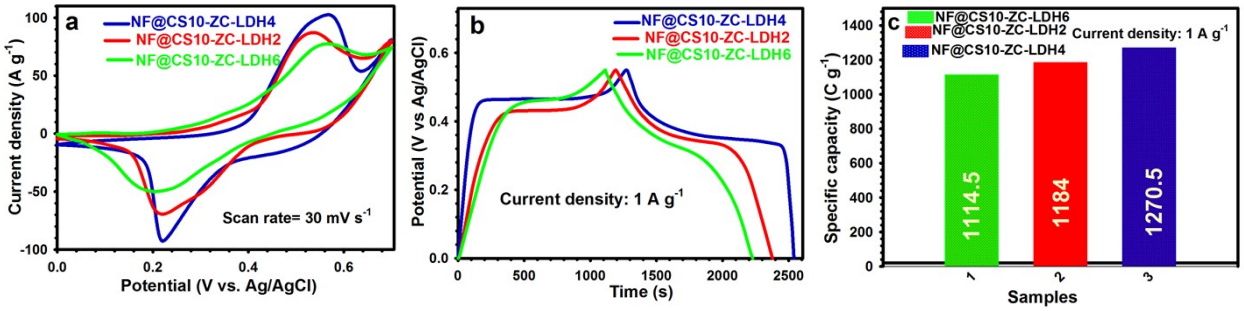

Fig. S7 (a) CV plots of the NF@CS5-ZC-LDH2, NF@CS5-ZC-LDH4, and NF@CS5-ZC-LDH6 electrodes at 30 mV s^{-1}. (b) GCD curves of the NF@CS5-ZC-LDH2, NF@CS5-ZC-LDH4, and NF@CS5-ZC-LDH6 electrodes at 1 A g^{-1}. (c) Specific capacities of the NF@CS5-ZC-LDH2, NF@CS5-ZC-LDH4, and NF@CS5-ZC-LDH6 electrodes at 1 A g^{-1}.

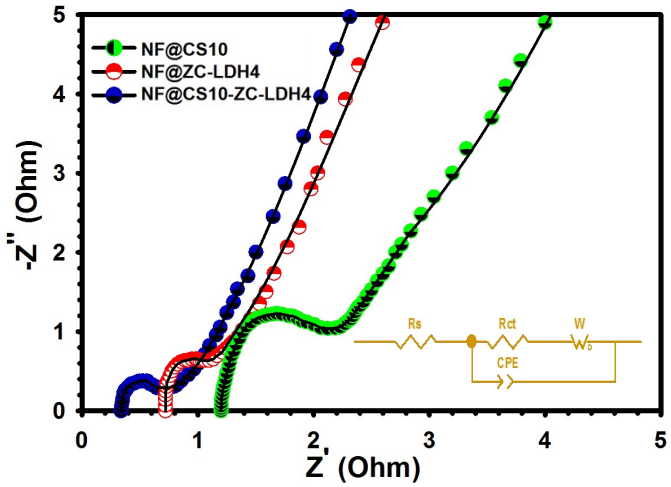

Fig. S8 Nyquist plots of the NF@CS10, NF@ZC-LDH4, and NF@CS10-ZC-LDH4 electrodes (inset indicate the equivalent circuit model and magnified Nyquist curves).

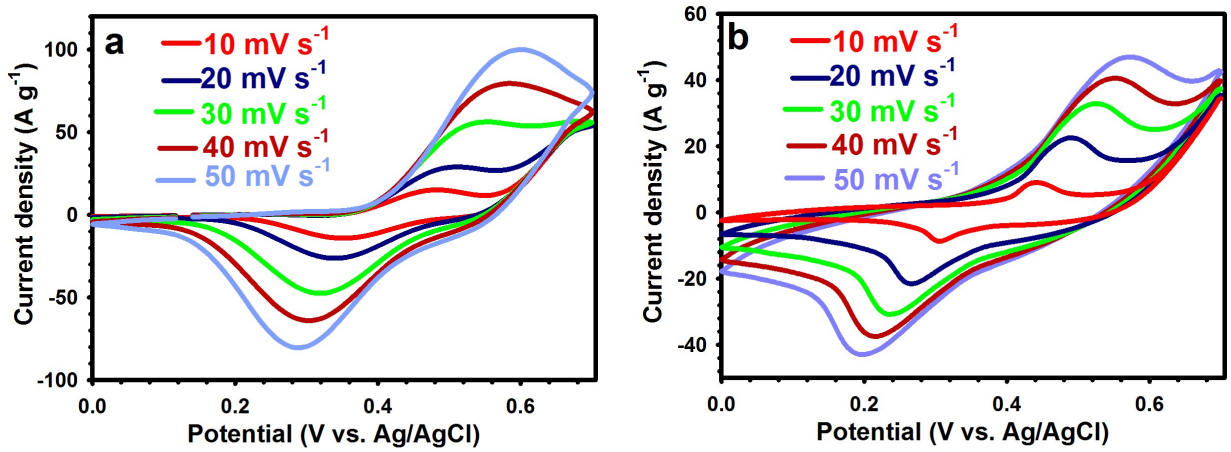

Fig. S9 (a) CV curves of the NF@ZC-LDH4 electrode at various scan rates from 10 to 50 mV s^{-1}. (b) CV curves of the NF@CS10 electrode at various scan rates from 10 to 50 mV s^{-1}.

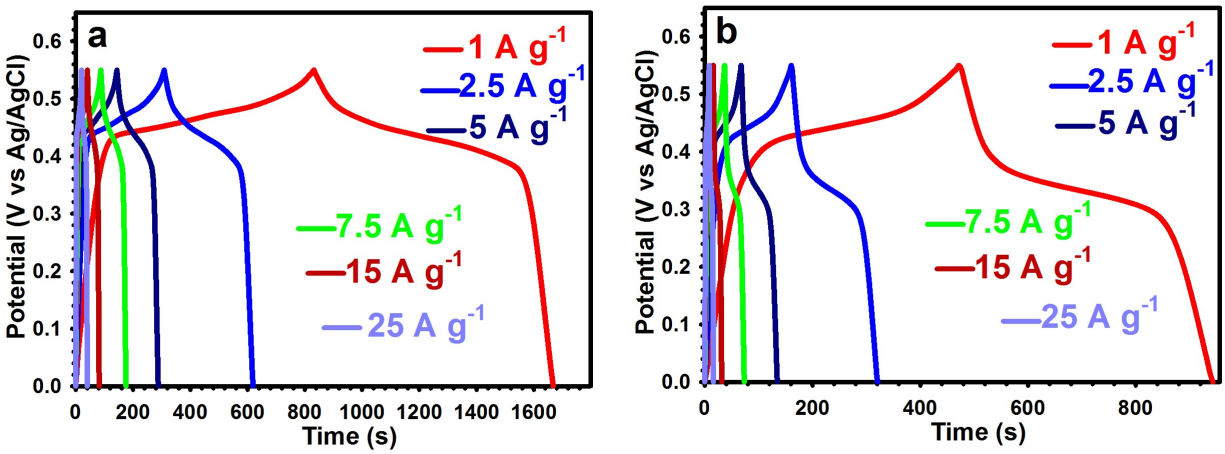

Fig. S10 (a) GCD curves of the NF@ZC-LDH4 electrode from 1 to 25 A g^{-1}. (b) GCD curves of the NF@CS10 electrode from 1 to 25 A g^{-1}.

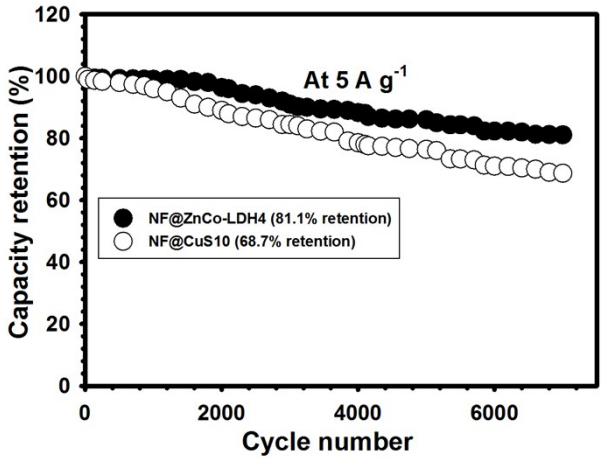

Fig. S11 Durability test of the NF@CuS10 and NF@ZC-LDH4 electrodes.

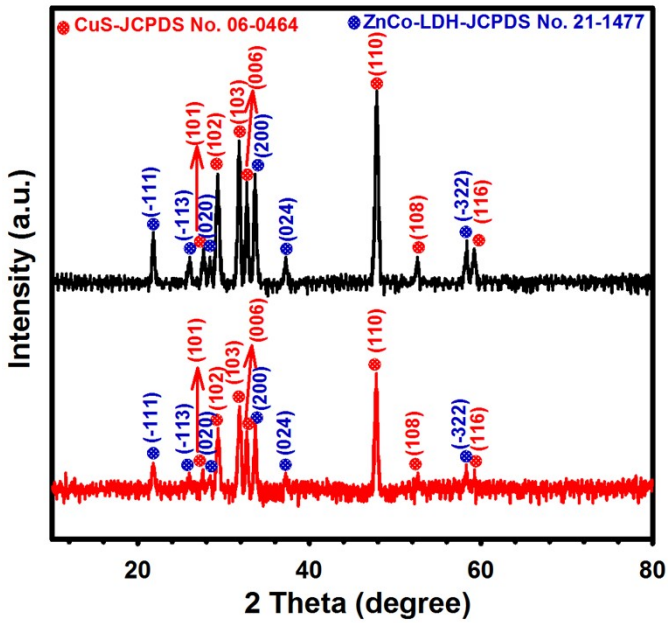

Fig. S12 XRD patterns of the CS10-ZC-LDH4 sample before and after durability test.

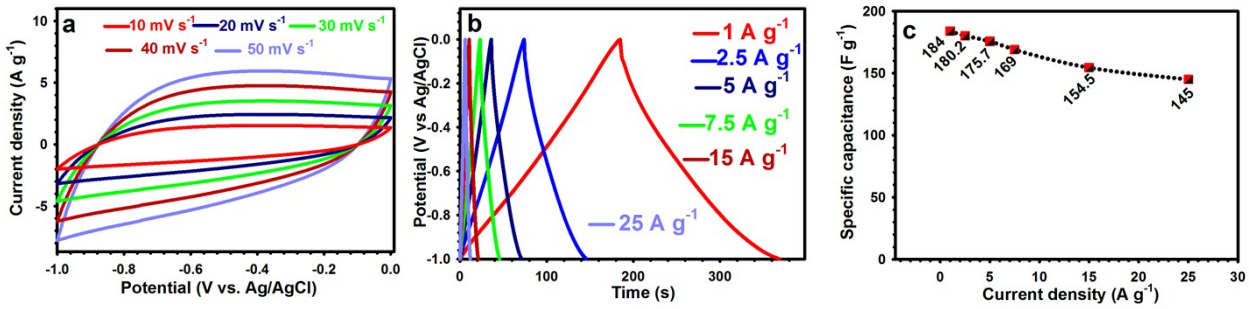

Fig. S13 (a) CV plots of the NF@AC at various scan rates from 10 to 50 mV s^{-1}. (b) GCD plots of the NF@AC@ at various current densities from 1 to 25 A g^{-1}. (c) Rate capability of the NF@AC electrode.

Table S1. Comparison of the performance of the NF@CS10-ZC-LDH4 with other previously reported materials.

Composition	Capacity (C/g)	Cycles, retention	Rate capability	ED (Wh kg^{-1})	Reference
CoNi-LDH	1031 at 1 A g^{-1}	50000, 88.2%	64.7% at 25 A g^{-1}	49	1
NiCoMn-S-1.5	657.7 at 1 A g^{-1}	50000, 90%	51.61% at 50 A g^{-1}	36.3	2
Co_9S_8	926 at 1 A g^{-1}	8000, 86%	67.4% at 15 A g^{-1}	25.49	3
$NiCo_2S_4$/HMCSs	659 at 1 A g^{-1}	3000, 90.1%	53.4% at 10 A g^{-1}	35.5	4
Co_3S_4/g-C_3N_4-10	415 at 0.5 A g^{-1}	5000, 75.6%	54.5% at 10 A g^{-1}	37.7	5
NiCoMn-S	661 at 1 A g^{-1}	1000, 86.45%	66.56% at 50 A g^{-1}	42.1	6
$CoNi_2S_4$	1158 at 1 A g^{-1}	8500, 84%	60.8% at 10 A g^{-1}	34.4	7
NiCo2S4/NGF	558 at 1 A g^{-1}	6000, 92.6%	55.5% at 20 A g^{-1}	36.8	8
NF@CS10-ZC-LDH4	1270.5 at 1 A g^{-1}	8000, 90.7 (3 E)	71.5% at 25A g^{-1}	62.4	This work

References

1. Z. Li, H. Mi, F. Guo, C. Ji, S. He, H. Li and J. Qiu, Oriented Nanosheet-Assembled CoNi-LDH Cages with Efficient Ion Diffusion for Quasi-Solid-State Hybrid Supercapacitors, *Inorg. Chem*. 2021, **60**, 12197–12205.

2. J. Zhang, C. Li, M. Fan, T. Ma, H. Chen and H. Wang, Two-dimensional nanosheets constituted trimetal Ni-Co-Mn sulfide nanoflower-like structure for high-performance hybrid supercapacitors, *Appl. Surf. Sci*. 2021, **565**, 150482.

3. J. Li, Q. Li, J. Sun, Y. Ling, K. Tao and L. Han, Controlled Preparation of Hollow and Porous Co_9S_8 Microplate Arrays for High-Performance Hybrid Supercapacitors, *Inorg. Chem*. 2020, **59**, 11174–11183.

4. Y. Liu, G. Jiang, Z. Huang, Q. Lu, B. Yu, U. Evariste and P. Ma, Decoration of Hollow Mesoporous Carbon Spheres by $NiCo_2S_4$ Nanoparticles as Electrode Materials for Asymmetric Supercapacitors, *ACS Appl. Energy Mater*. 2019, **2**, 8079–8089

5. W. Li, Y. Li, C. Yang, Q. Ma, K. Tao and L. Han, Fabrication of 2D/2D nanosheet heterostructures of ZIF-derived Co_3S_4 and g-C_3N_4 for asymmetric supercapacitors with superior cycling stability, *Dalton Trans* 2020, **49**, 14017–14029.

6. J. Cao, Y. Hu, Y. Zhu, H. Cao, M. Fan, C. Huang, K. Shu, M. He and H. C. Chen, Synthesis of mesoporous nickel-cobalt-manganese sulfides as electroactive materials for hybrid supercapacitors, *Chem. Eng. J* 2021, **405**, 126928.

7. X. Zhao, Q. Ma, K. Tao and L. Han, ZIF-Derived Porous $CoNi_2S_4$ on Intercrosslinked Polypyrrole Tubes for High-Performance Asymmetric Supercapacitors, *ACS Appl. Energy Mater*. 2021, **4**, 4199–4207.

8. Y. Chen, T. Liu, L. Zhang and J. Yu, $NiCo_2S_4$ Nanotubes Anchored 3D Nitrogen-Doped Graphene Framework as Electrode Material with Enhanced Performance for Asymmetric Supercapacitors, *ACS Sustainable Chem. Eng*. 2019, **7**, 11157–11165.